A COMPUTATIONAL STUDY ON A NATURE INSPIRED NOVEL DOUBLY CURVED FOLDED SHELL STRUCTURAL FORM

SUHAIL ABDULAZIZ ABDULRAZZACK

UNIVERSITI SAINS MALAYSIA

2007

A COMPUTATIONAL STUDY ON A NATURE INSPIRED NOVEL DOUBLY CURVED FOLDED SHELL STRUCTURAL FORM

by

SUHAIL ABDULAZIZ ABDULRAZZACK

Thesis submitted in fulfilment of the requirements
for the degree of
Doctor of Philosophy

December 2007

ACKNOWLEDGEMENTS

Everyday we all see thousands of objects in nature, but very few try to learn from these objects for possible applications related to their disciplines. Assoc. Prof. Dr. Choong Kok Keong, the first supervisor, is the man behind the beautiful idea of this research. I would like to extend my sincere gratitude to Assoc. Prof. Dr. Choong for his invaluable advice, helpful discussions, constant support and encouragement throughout the research work. I admire his professional style at both the academic as well as the personal level.

Sincere thanks to Assoc. Prof. Dr. Taksiah A.Majid, the second supervisor, for helping me in the initial stages to locate and decide upon the research topic and for her advice in the academic as well as the administrative matters related to this research.

I am grateful to my beloved family in Yemen for their prayer and moral support. Special thanks to my father Mr. A.Aziz Razzack and my uncle Mr. A.Rashid A.Razzack; without their moral and financial support it would not have been possible to successfully complete this research. I would also like to thank my wife and children for their prayer, patience and moral support.

I would also like to thank the School of Civil Engineering for giving me the opportunity to carry out my PhD research work. I sincerely thank the School's staff who directly or indirectly helped me. Special thanks to Assoc. Prof. Dr. Wan Muh. Aminuddin and Assoc. Prof. Dr. Mohd Sanusi for their invaluable advice in deciding upon the research topic.

I am, also, thankful to the School of Biology and School Housing Building and Planning for allowing me to use their facilities. Sincere thanks to the laboratory technicians of both schools for their support in the practical part of the research.

Finally, a word of thanks and appreciation to all my friends who directly or indirectly helped me during the different stages of the research. In this respect, I would like to thank Mr. Ahmed Salem Al-Eraqi, Mr. Ismail A.Lateef, Mr. Lawan Suleiman, Mr. Salman Al-Shami, Mr. Waddah Munassar and Mr. Yasser Al-Saqqaf.

TABLE OF CONTENTS

	Page
ACKNOWLEDGEMENTS	ii
TABLE OF CONTENTS	iii
LIST OF TABLES	ix
LIST OF FIGURES	xii
LIST OF ABBREVIATION	xxv
LIST OF SYMBOLS	xxvi
ABSTRAK	xxviii
ABSTRACT	xxx
CHAPTER 1 : INTRODUCTION	**1**
1.1 General	1
1.2 Background of the Study	3
1.2.1 Structures Inspired from Non-Biological Systems	5
1.2.2 Structures Inspired from Biological Systems	6
1.3 Inspiring Source from Plants in Nature	7
1.4 The *Johannesteijsmannia altifrons*	8
1.5 Problem Statement	12
1.6 Research Objectives	12
1.7 Scope of Research	13
1.8 Thesis Layout	14
CHAPTER 2 : LITERATURE REVIEW	**16**
2.1 Shell Structures	16
2.1.1 Shell Structures in Nature	16
2.1.2 Characteristics of Surface Structures	19
2.1.3 Advantages of Shell Structures	21
2.1.4 Behaviour of Shell Structures	22
2.1.5 Classification of Shell Systems	23
2.2 Folded Surface and Plate Structures	27
2.2.1 Types of Folded Surface and Plate Structures	32
2.2.2 Folded Plate Hypar Shells	43
2.2.3 Behaviour of Folded Plate Structures	47
2.3 Research Status and Recent Works on Folded Plate Structures	55
2.4 Related Work	61

2.5 Closing Remarks 62

CHAPTER 3 : SOURCE REFERENCED CLASSIFICATION OF BIOMIMICRY 63

3.1 Introduction 63

3.2 Biomimicry 66

3.2.1 Definition of Biomimicry 67

3.2.2 Benefit of Biomimicry 67

3.3 Biomimicry: A Systematic Approach 69

3.3.1 Examples from the World of Plants 70

3.3.1.1 Deployable Shapes and Structures in Nature 70

3.3.1.2 Mimicking Photosynthesis 70

3.3.1.3 Efficient Natural Structures 71

3.3.2 Examples from the World of Animals 71

3.3.2.1 Active Deployable Camouflage 71

3.3.2.2 Automatic Assembly 71

3.3.2.3 Biomimetic Structures for LOComotion in the Human body (BIOLOCH) 72

3.3.2.4 Mimicking Social Insect Building 72

3.4 Biomimicry: A Classified Approach 73

3.4.1 Innovation Inspired by Nature 73

3.4.2 Biomimicry Technology Tree of the European Space Agency 73

3.4.3 Incorporation of Biology into Non-Biological Solution Platform – Biomimicry and TRIZ 74

3.5 Source Referenced Classification (SRC) 76

3.5.1 Basic Framework of Source Referenced Classification 79

3.5.2 Examples on Source Referenced Classification 81

3.5.2.1 Colour Change in Animals – Natural Camouflage Systems 81

3.5.2.2 Deployable Structures – Folding Systems in Nature 83

3.5.2.3 Structural Efficiency and Architectural Beauty – Shells in Nature 85

3.5.3 Multifunctional Source Referenced Classification of Biomimicry 88

3.5.4 Foreseen Merits of Source Referenced Classification 89

3.6 Closing Remarks 91

CHAPTER 4 : SURFACE MEASUREMENT OF THE JOHANNESTEIJSMANNIA ALTIFRONS 92

4.1 Introduction 92

4.2 Structured Lighting Method – Conventional Approach 94

4.3 Parallax Effect and Distortion 98
4.4 Modified Coordinates Calculation Approach 102
4.5 Two Point Triangulation (TPT) Method for 3D Surface Measurement 109
4.6 Verification Models and Associated Distortion of Images 113
4.6.1 Fabrication of the Verification Models 115
4.6.2 Actual Surface Data of the Verification Models 116
4.6.2.1 Actual Surface Data Acquisition of Verification Models 1 and 2 116
4.6.2.2 Actual Surface Data Acquisition of Verification Model 3 118
4.6.2.3 Remarks on the Application of TPT Approach 123
4.6.3 Distorted Images of the Verification Models 126
4.7 Evaluation of the Measurement Results 132
4.7.1 Result Evaluation for Verification Model 1: Flat Folded Model 132
4.7.1.1 Coordinates Analysis in *x*-Direction – Model 1 137
4.7.1.2 Distance Analysis in *x*-Direction – Model 1 139
4.7.1.3 Coordinates Analysis in *y*-Direction along Ridge/Valley Lines – Model 1 141
4.7.1.4 Distance Analysis in *y*-Direction – Model 1 144
4.7.1.5 Coordinates Analysis in *z*-Direction – Model 1 148
4.7.1.6 Remarks on Measurement Results of Model 1 150
4.7.2 Results Evaluation for Verification Model 2: Singly Curved Folded Model 152
4.7.2.1 Coordinates Analysis in *x*-Direction – Model 2 156
4.7.2.2 Distance Analysis in *x*-Direction – Model 2 158
4.7.2.3 Coordinates Analysis in *y*-Direction Along Ridge/Valley Lines – Model 2 160
4.7.2.4 Distance Analysis in *y*-Direction – Model 2 163
4.7.2.5 Coordinates Analysis in *z*-Direction – Model 2 167
4.7.2.6 Remarks on Measurement Results of Model 2 169
4.7.3 Results Evaluation for Verification Model 3: Doubly Curved Folded Model 171
4.7.3.1 Distance Analysis along Left Zigzag Edge – Model 3 173
4.7.3.2 Distance Analysis along Right Zigzag Edge – Model 3 175
4.7.3.3 Distance Analysis along Central Zigzag – Model 3 177
4.7.3.4 Distance Analysis along Ridge and Valley Lines – Model 3 Left Half 179
4.7.3.5 Distance Analysis along Ridge and Valley Lines – Model 3 Right Half 181
4.7.3.6 Combined Distance Analysis- Model 3 183

4.7.3.7 Remarks on Measurement Results of Model 3 183
4.8 Surface Data Acquisition of the Leaves of *Johannesteijsmannia altifron* 188
4.8.1 Measurement Results of the Surface of *J. altifrons* 191
4.8.1.1 Surface Smoothening of *J. altifrons* Models – Leaves (A) and (B) 194
4.9 Closing Remarks 199

CHAPTER 5 : GENERATION OF SHELL SURFACES WITH FOLDS 200
5.1 Introduction 200
5.2 Generation of Doubly Curved Folded Surfaces Using Pure or Rigid Geometry Approach 201
5.2.1. Generation of Doubly Curved Folded Surfaces Using Rigid Geometry Approach with Rotation about One Diagonal 201
5.2.2 Generation of Doubly Curved Folded Surfaces Using Rigid Geometry Approach with Rotation about Both Diagonals 209
5.3 Generation of Doubly Curved Folded Surfaces Using Natural Geometry Approach 214
5.4 Further Applications 221
5.5 Closing Remarks 226

CHAPTER 6 : MODELING AND ANALYSIS OF SHELL SURFACES WITH FOLDS - NATURAL FORMS 228
6.1 Introduction 228
6.2 Geometrical Modeling of the Leaf 229
6.2.1 Geometrical Modeling of the Leaf Surface 229
6.2.2 Geometrical Modeling of the Stem 234
6.2.2.1 The Transition Zone 236
6.2.3 Final Representative/Typical Leaf Model 238
6.3 Geometrical Modeling of the Flattened Leaf 241
6.4 Section Properties of the Stem 247
6.4.1 Measurement of the Stem Cross-Sections 248
6.4.2 Calculation of the Stem Cross-Sections' Properties 253
6.5 Density of the Leaf 260
6.5.1 Stem Density 260
6.5.2 Density of the Folded Leaf Surface 262
6.6 Analysis of the *J. altifrons* 265
6.6.1 Types of Elements Used in Modeling the *J. altifrons* 266
6.6.1.1 Beam Element 266

6.6.1.2 Plate Element 268
6.6.2 Material Properties 273
6.6.3 Performance of the Transition Zone – Trial Analysis 277
6.6.4 Analysis and Results of the *J. altifrons* – Leaf (A) 284
6.6.4.1 Finite Element Model of Leaf (A) 284
6.6.4.2 Section Properties of Beam Elements – Stem of Leaf (A) 286
6.6.4.3 Thickness Variation of Plate Elements of the Surface and Transition Zone – Leaf (A) 286
6.6.4.4 Loading, Boundary Conditions and Type of Analysis 286
6.6.4.5 Results of FEA - Leaf (A) 289
6.6.5 Analysis and Results of the *J. altifrons* – Leaf (B) 303
6.6.5.1 Finite Element Model of Leaf (B) 303
6.6.5.2 Section Properties of Beam Elements – Stem of Leaf (B) 305
6.6.5.3 Thickness Variation of Plate Elements of the Surface and Transition Zone – Leaf (B) 305
6.6.5.4 Loading, Boundary Conditions and Type of Analysis 305
6.6.5.5 Results of FEA - Leaf (B) 308
6.6.6 Discussion of the Results 322
6.6.6.1 Displacement 332
6.6.6.2 Plate Forces and Moments 332
6.6.6.3 Plate Stresses 334
6.6.6.4 Stem Forces and Moments 335
6.6.6.5 Stem Stresses 337
6.7 Closing Remarks 338

CHAPTER 7 : MODELING AND ANALYSIS OF SHELL SURFACES WITH FOLDS – NATURE INSPIRED PRACTICAL FORMS 340

7.1 Introduction 340
7.2 Generation of the Models 341
7.2.1 Modeling the Folded Surface 341
7.2.2 Modeling the Stem 345
7.2.3 Final Analysis Models 346
7.3 Material Properties 350
7.4 Loading, Boundary Conditions and Type of Analysis 350
7.5 Results of FEA – Practical Forms 350
7.5.1 Results of FEA - 4 Folds Models 351
7.5.2 Results of FEA - 6 Folds Models 352

7.6 Discussion of the Results 353
7.6.1 Displacement 353
7.6.2 Moments 354
7.6.2.1 Folded Surface Moments 354
7.6.2.2 Stem Moments 356
7.6.3 Stresses 356
7.6.3.1 Stresses on the Folded Surface 357
7.6.3.2 Stem Stresses 359
7.7 Closing Remarks 360

CHAPTER 8 : CONCLUSIONS AND RECOMMENDATIONS 362
8.1 Conclusions 362
8.2 Recommendations 367

REFERENCES 368

APPENDICES
Appendix A: Stiffness Comparison of Folded Versus Flat Plate 377
Appendix B: Coordinates Determination of Camera Focus 381
Appendix C: Coordinates Determination of Projector Focus 384
Appendix D: Folded Surface Density – Leaves (A) and (B) 389
Appendix E: Section Properties of Stem's Beam Elements – Leaf (A) 391
Appendix F: Thickness of Plate Elements – Leaf (A) 395
Appendix G: Section Properties of Stem's Beam Elements – Leaf (B) 397
Appendix H: Thickness of Plate Elements – Leaf (B) 401
Appendix I: Results of FEA of Leaf (A) – Folded Model 403
Appendix J: Results of FEA of Leaf (A) – Flattened Model 410
Appendix K: Results of FEA of Leaf (B) – Folded Model 417
Appendix L: Results of FEA of Leaf (B) – Flattened Model 424
Appendix M: Results of FEA – 4 Folds Models 431
Appendix N: Results of FEA – 6 Folds Models 450

PUBLICATIONS 469

LIST OF TABLES

		Page
Table 2.1	Shell Structures Classification by Geometry	26
Table 4.1	Error in TPT Results for Profiles 1, 2 and 3 of Verification Model 2	120
Table 4.2	Summary of Frequency Distribution Analysis of Error in TPT – Model 2	122
Table 4.3	Scale Factors of the Images for the Verification Models 1, 2 and 3	126
Table 4.4	Sample Calculation Based on Conventional Approach along Fringe 1 – Model 1	134
Table 4.5	Sample Calculation Based on Proposed Approach along Fringe 1 – Model 1	135-136
Table 4.6	Distance Analysis in *x*-Direction along Fringe 1 – Model 1	140
Table 4.7	Distance Analysis along Ridge and Valley Lines – Model 1	147
Table 4.8	Summary of Frequency Distribution of Errors in *z*-Coordinate Values – Model 1	148
Table 4.9	Dimensions of Verification Model 1 before and after Applying the Proposed Algorithm	151
Table 4.10	Sample Calculation Based on Conventional Approach along Fringe 5 – Model 2	153
Table 4.11	Sample Calculation Based on Proposed Approach along Fringe 5 – Model 2	154-155
Table 4.12	Distance Analysis along Fringe 5 – Model 2	159
Table 4.13	Distance Analysis along Ridge and Valley Lines – Model 2	166
Table 4.14	Summary of Frequency Distribution of Errors in *z*-Coordinate Values – Model 2	167
Table 4.15	Dimensions of Verification Model 2 before and after Applying the Proposed Algorithm	170
Table 4.16	Distance Analysis along Left Zigzag Edge – Model 3	173
Table 4.17	Distance Analysis along Right Zigzag Edge of Model 3	175
Table 4.18	Distance Analysis along Central Zigzag Line of Model 3	177
Table 4.19	Distance Analysis along Ridge/Valley Lines on Left Half of Model 3	179
Table 4.20	Distance Analysis along Ridge/Valley Lines on Right Half of Model 3	181
Table 4.21	Dimensions of Reconstructed Models of *J. altifrons* Leaves (A) and (B) before and after Applying the Proposed Algorithm	191
Table 6.1	Sample Locations along the Leave' Stems	247

Table 6.2	Summary of Section Properties Results for Leaf (A) at the 10 Measured Sections	256
Table 6.3	Summary of Section Properties Results for Leaf (B) at the 10 Measured Sections	256
Table 6.4	Stem Density – Leaf (A)	261
Table 6.5	Stem Density – Leaf (B)	261
Table 6.6	Density Results of Leaf (A) and Leaf (B) in Statistical Terms	264
Table 6.7	Properties of Wood Species Used as Input Data in Leaves Analysis	275
Table 6.8	Reference Strength Values of Wood Species Used in the Analysis	276
Table 6.9	Performance Evaluation of the Transition Zone for Analysis Set 1 - Displacement of Nodes along Fringe Lines 11, 38 and 59	282
Table 6.10	Shape and Type of Elements Used in Modeling Leaf (A)	285
Table 6.11	Description of Leaf (A) – Folded Model	285
Table 6.12	Description of Leaf (A) - Flattened Model	285
Table 6.13	Displacement Results of Folded and Flattened Models of Leaf (A) for 11 Species of Wood	290
Table 6.14	Maximum and Minimum Plate Stresses (σ_x) at the Top Surface of the Folded and Flattened Versions of Leaf (A)	291
Table 6.15	Maximum and Minimum Plate Stresses (σ_x) at the Bottom Surface of the Folded and Flattened Versions of Leaf (A)	292
Table 6.16	Maximum and Minimum Plate Stresses (σ_y) at the Top Surface of the Folded and Flattened Versions of Leaf (A)	293
Table 6.17	Maximum and Minimum Plate Stresses (σ_y) at the Bottom Surface of the Folded and Flattened Versions of Leaf (A)	294
Table 6.18	Displacement Results of the Stem of the Folded and Flattened Models of Leaf (A)	295
Table 6.19	Shape and Type of Elements Used in Modeling Leaf (B)	303
Table 6.20	Description of Leaf (B) - Folded Model	304
Table 6.21	Description of Leaf (B) – Flattened Model	304
Table 6.22	Displacement Results of Folded and Flattened Models of Leaf (B) for 11 Species of Wood	309
Table 6.23	Maximum and Minimum Plate Stresses (σ_x) at the Top Surface of the Folded and Flattened Versions of Leaf (B)	310
Table 6.24	Maximum and Minimum Plate Stresses (σ_x) at the Bottom Surface of the Folded and Flattened Versions of Leaf (B)	311
Table 6.25	Maximum and Minimum Plate Stresses (σ_y) at the Top Surface of the Folded and Flattened Versions of Leaf (B)	312
Table 6.26	Maximum and Minimum Plate Stresses (σ_y) at the Bottom Surface of the Folded and Flattened Versions of Leaf (B)	313

Table 6.27	Displacement Results of the Stem of the Folded and Flattened Models of Leaf (B)	314
Table 6.28	Summary of Maximum Deflection of Leaves (A) and (B)	323
Table 6.29	Summary of Maximum Tensile and Compressive Plate Stress (σ_x) at Top – Leaves (A) and (B)	324
Table 6.30	Summary of Maximum Tensile and Compressive Plate Stress (σ_x) at Bottom – Leaves (A) and (B)	325
Table 6.31	Summary of Maximum Tensile and Compressive Plate Stress (σ_y) at Top – Leaves (A) and (B)	326
Table 6.32	Summary of Maximum Tensile and Compressive Plate Stress (σ_y) at Bottom – Leaves (A) and (B)	327
Table 6.33	Maximum Stresses (σ_x) at Top in Folded Versions of the Leaves Expressed as Percentage of Corresponding Stresses in the Flattened Versions – Leaves (A) and (B)	328
Table 6.34	Maximum Stresses (σ_x) at Bottom in Folded Versions of the Leaves Expressed as Percentage of Corresponding Stresses in the Flattened Versions – Leaves (A) and (B)	329
Table 6.35	Maximum Stresses (σ_y) at Top in Folded Versions of the Leaves Expressed as Percentage of Corresponding Stresses in the Flattened Versions – Leaves (A) and (B)	330
Table 6.36	Maximum Stresses (σ_y) at Bottom in Folded Versions of the Leaves Expressed as Percentage of Corresponding Stresses in the Flattened Versions – Leaves (A) and (B)	331
Table 7.1	Description of 10x Scaled-Up 4 Folds Models	347
Table 7.2	Description of 10x Scaled-Up 6 Folds Models	347
Table 7.3	Summary of Folded Surface Results – 4 Folds Models	351
Table 7.4	Summary of Stem Results – 4 Folds Models	351
Table 7.5	Summary of Folded Surface Results – 6 Folds Models	352
Table 7.6	Summary of Stem Results – 6 Folds Models	352
Table A1	Comparison of Moment of Inertia Values of Folded versus Flat Plate	380
Table D1	Folded Surface Density – Leaf (A)	389
Table D2	Folded Surface Density – Leaf (B)	390
Table E1	Section Properties of all Tapered Beam Elements along the Stem of Leaf (A)	391-394
Table F1	Plate Elements' Group Thickness – Leaf (A)	395-396
Table G1	Section Properties of all Tapered Beam Elements along the Stem of Leaf (B)	397-400
Table H1	Plate Elements' Group Thickness – Leaf (B)	401-402

LIST OF FIGURES

		Page
Fig. 1.1	Some Successful Shell Applications	2
Fig. 1.2	The Magnificent Palm – *Johannesteijsmannia altifrons*	10
Fig. 1.3	Heights Reached by the *Johannesteijsmannia altifrons*	11
Fig. 1.4	Picture Showing Serrated Edge and Fold Lines on the *Johannesteijsmannia altifrons*	11
Fig. 2.1	Surfaces in Nature	18
Fig. 2.2	In-Plane and Out of Plane Forces on a Shell Element	23
Fig. 2.3	Definition of Curvature	24
Fig. 2.4	Shell Forms	25
Fig. 2.5	Folded Plate Structures	27
Fig. 2.6	Concrete Airship Hangar, Orly, France 1924	28
Fig. 2.7	Exhibition Building, Turin, Italy 1948	29
Fig. 2.8	TWA Hangar, Kansas City, USA 1956	30
Fig. 2.9	Super-bay Hangar, Los Angeles, USA 1971	30
Fig. 2.10	American Airlines Hangar, San Francisco, USA 1971	31
Fig. 2.11	Assembly Hall, University of Illinois, Illinois, USA 1962	31
Fig. 2.12	Folded Plate Structure Systems	33
Fig. 2.13	Folded Plate Structures	34
Fig. 2.14	UNESCO Headquarters, Paris, France 1957	35
Fig. 2.15	ACI Headquarters, Detroit, Michigan, USA 1958	35
Fig. 2.16	Christ Church, Bochum, Germany 1959	36
Fig. 2.17	Customs Building, Glanerburg, the Netherlands 1959	37
Fig. 2.18	Den Helder Station, the Netherlands 1959	37
Fig. 2.19	Verenigd Plastic - Verkoopkantoor N. V. Laboratory, Zeist, the Netherlands 1960	38
Fig. 2.20	St. John's Abby Church, Collegeville, Minnesota, USA 1961	39
Fig. 2.21	Air Force Academy Chapel, Colorado Springs, Colorado, USA 1961	39
Fig. 2.22	Gunma Music Center, Takasaki, Japan 1961	40
Fig. 2.23	Church of Hoensbroek, the Netherlands 1964	40
Fig. 2.24	Saint Pius Church, Rock Island, USA 1964	41
Fig. 2.25	Auditorium Model, Delft Polytechnic School, the Netherlands 1966	41
Fig. 2.26	Sarasota Herals -Tribune's Headquarters, Florida, USA	42

Fig. 2.27	Shallow Umbrella Shell for a Warehouse, Mexico City, Mexico	44
Fig. 2.28	12 m Cantilever Entrance to Lederle Laboratories, Mexico City, Mexico	45
Fig. 2.29	Bandshell, Santa Fe Housing Project, Mexico City, Mexico	45
Fig. 2.30	Subway Station, Mexico City, Mexico	46
Fig. 2.31	Signpost for Housing Development in Tequesquitenge, Mexico City, Mexico	46
Fig. 2.32	Longitudinal Action of Folded-Plate Structures	48
Fig. 2.33	Transverse Action of Folded-Plate Structures	48
Fig. 2.34	Special Conditions of Folded Plates	51
Fig. 2.35	Folded Plate Action in the Transverse Direction	52
Fig. 2.36	Folded Plate Action in the Longitudinal Direction	53
Fig. 2.37	Finite Elements and Various Topics in Analysis of Various Structures	56
Fig. 3.1	Proposed Approach of Source Referenced Classification of Biomimicry	77
Fig. 3.2	Taxonomy of Living Things on Earth	79
Fig. 3.3	Basic Framework of Source Referenced Classification	80
Fig. 3.4	SRC – Natural Camouflage Systems (Colour Change in Animals)	82
Fig. 3.5	SRC – Deployable Structures (Folding Systems in Nature)	84
Fig. 3.6	SRC – Structural Efficiency and Architectural Beauty (Shells in Nature)	86
Fig. 3.7	Combination of Folding/Unfolding Property and Structural Properties in Three-Banded Armadillos	88
Fig. 4.1	Principle of Fringe Projection Method	96
Fig. 4.2	A simplified Example of Parallax	99
Fig. 4.3	Parallax Distortion	99
Fig. 4.4	Sign Convention for Coordinate Correction of Points on Image in *xy*-Plane	99
Fig. 4.5	Effect of Object Size on Image Distortion	101
Fig. 4.6	Geometry of Proposed Approach	104
Fig. 4.7	Geometry of Two Point Triangulation	112
Fig. 4.8	Verification Model 1 (Flat Folded Surface)	114
Fig. 4.9	Verification Model 2 (Singly Curved Folded Surface)	114
Fig. 4.10	Verification Model 3 (Doubly Curved Folded Surface)	114
Fig. 4.11(a)	Model 1 (Front View)	117
Fig. 4.11(b)	Profile of Verification Model 1 (Section A – A)	117

Fig. 4.12(a)	Model 2 (Front View)	117
Fig. 4.12(b)	Profile of Verification Model 2 (Section B – B)	117
Fig. 4.13	Locations of Measured Profiles on Model 2 by TPT Method	119
Fig. 4.14	TPT Setup for Measurement of Verification Model 2	119
Fig. 4.15	Measured Profiles by TPT Method versus Reference Profile on Model 2	121
Fig. 4.16	Illustration of the Doubly Curved Surface of Verification Model 3	124
Fig. 4.17	TPT Setup for Measurement of Verification Model 2	124
Fig. 4.18	Reconstructed Line, Meshed and Rendered Versions of Model 3 Based on TPT Results	124
Fig. 4.19(a)	Front View of Model 3	125
Fig. 4.19(b)	Actual Profile of Verification Model 3 (Section C - C)	125
Fig. 4.19(c)	Actual Profile of Verification Model 3 (Section D - D)	125
Fig. 4.20	Verification Model 1 with Projected Fringes	127
Fig. 4.21	Verification Model 2 with Projected Fringes	127
Fig. 4.22	Verification Model 3 with Projected Fringes	127
Fig. 4.23	Comparison of Distorted Shape versus Actual Shape of Verification Model 1	128
Fig. 4.24	Comparison of Distorted Shape versus Actual Shape of Verification Model 2	129
Fig. 4.25	Comparison of Distorted Shape versus TPT Shape of Verification Model 3	130
Fig. 4.26	Labeling of Model 1 for Measurement Evaluation Analysis	133
Fig. 4.27	Error Variation in *x*-Coordinate Values along Fringe 1 – Model 1	137
Fig. 4.28	Error in Distances Obtained from Conventional and Proposed Approaches with Respect to Actual Distances on Model 1 along Fringe 1	140
Fig. 4.29	Error Variation in *y*-Coordinate Values along Valley Line V1 and Ridge Line R10 - Model 1	143
Fig. 4.30	Plot of Difference between *y*-Coordinate Values of Conventional and Proposed Approaches ($y_C - y_P$) along Ridge Line R1 versus *y*-Coordinate Values of Conventional Approach (y_C) – Model 1	145
Fig. 4.31	Error in Distances Obtained from Conventional and Proposed Approaches with Respect to Actual Distances on Model 1 along Fringe 1	147
Fig. 4.32(a)	Frequency Distribution of Errors in *z*-Coordinate Values, Conventional Approach - Model 1	149
Fig. 4.32(b)	Frequency Distribution of Errors in *z*-Coordinate Values, Proposed Approach - Model 1	149

Fig. 4.33	Comparison of Conventional/Proposed Approach Shapes versus Actual Shape – Model 1	151
Fig. 4.34	Labeling of Model 2 for Comparison Analysis	152
Fig. 4.35	Error Variation in *x*-Coordinate Values along Fringe 5 – Model 2	156
Fig. 4.36	Error in Distances Obtained from Conventional and Proposed Approaches with Respect to Actual Distances on Model 2 along Fringe 5	159
Fig. 4.37	Error Variation in *y*-Coordinate Values along Valley Line V5 and Ridge Line R9 - Model 2	162
Fig. 4.38	Plot of Difference between *y*-Coordinate Values of Conventional and Proposed Approach ($y_C - y_P$) along Ridge Line R1 versus *y*-Coordinate Values of Conventional Approach (y_C) – Model 2	164
Fig. 4.39	Error in Distances from Conventional and Proposed Approaches with Respect to Actual Distances on Model 2 along Ridge and Valley Lines	166
Fig. 4.40(a)	Frequency Distribution of Errors in *z*-Coordinate Values, Conventional Approach - Model 2	168
Fig. 4.40(b)	Frequency Distribution of Errors in *z*-Coordinate Values, Proposed Approach - Model 2	168
Fig. 4.41	Comparison of Conventional/Proposed Approach Shapes versus Actual Shape – Model 2	170
Fig. 4.42	Labeling of Model 3 for Comparison Analysis	172
Fig. 4.43	Errors in Distances Measured along Left Zigzag Edge AD of Model 3	174
Fig. 4.44	Errors in Distances Measured along Right Zigzag Edge CD of Model 3	176
Fig. 4.45	Errors in Distances Measured along Central Zigzag Line BD of Model 3	178
Fig. 4.46	Errors in Distances Measured along Ridge/Valley Lines on Left Half of Model 3	180
Fig. 4.47	Errors in Distances Measured along Ridge/Valley Lines on Right Half of Model 3	182
Fig. 4.48	Errors in Distances Measurement Considering the Combined Data Sets of Model 3	184
Fig. 4.49(a)	Wire Frame Isometric Views of Calibration Model 3 Obtained from the Conventional Approach, the Proposed Approach and TPT Method	185
Fig. 4.49(b)	Rendered Isometric Views of Calibration Model 3 Obtained from the Conventional Approach, the Proposed Approach and TPT Method	185
Fig. 4.50	Comparison of Conventional/Proposed Approach Shapes versus TPT Shape – Model 3	186

Fig. 4.51	Orientation of Final Model 3 with respect to the Captured Image	187
Fig. 4.52	Imaging Setup for 3D Data Acquisition of the Surface of *J. altifrons*	188
Fig. 4.53	Image of Leaf (A) with Fringe Projections	189
Fig. 4.54	Image of Leaf (B) with Fringe Projections	189
Fig. 4.55	*J. altifrons* Leaf (A) Model based on the Conventional Approach	192
Fig. 4.56	*J. altifrons* Leaf (A) Model based on the Proposed Approach	192
Fig. 4.57	*J. altifrons* Leaf (B) Model based on the Conventional Approach	193
Fig. 4.58	*J. altifrons* Leaf (B) Model based on the Proposed Approach	193
Fig. 4.59	Kinks Smoothening along Ridge and Valley Lines	195
Fig. 4.60	Plot of *z* versus *y*-Coordinates along Fold Line 10 of Leaf (B) before and after Smoothening	196
Fig. 4.61	Frequency Distribution of error in *z*-Coordinate Values along Fold Line 10 – Leaf (B)	196
Fig. 4.62	Meshed and Rendered Models of Leaf (A)	197
Fig. 4.63	Meshed and Rendered Models of Leaf (B)	198
Fig. 5.1	Step 1 – Starting Geometrical Shape ‘Plane Rhombus’: Rigid Geometry with Rotation about One Axis	202
Fig. 5.2	Step 2 – Rotation of Two Adjacent Sides: Rigid Geometry with Rotation about One Axis	202
Fig. 5.3	Step 3 – Generating Doubly Curved Surface by Meshing the Space Rhombus: Rigid Geometry with Rotation about One Axis	204
Fig. 5.4	Step 4 – Generation of Curved Diagonals on the Doubly Curved Surface: Rigid Geometry with Rotation about One Axis	204
Fig. 5.5	Step 5 – Generation of Identical Doubly Curved Surface through Shifting: Rigid Geometry with Rotation about One Axis	205
Fig. 5.6	Step 6 – Generation of the Zigzag Boundary: Rigid Geometry with Rotation about One Axis	205
Fig. 5.7	Step 7 – Generation of Folds: Rigid Geometry with Rotation about One Axis	206
Fig. 5.8	Rendered Views of the Generated Model: Rigid Geometry with Rotation about One Diagonal	207
Fig. 5.9	Possible Shapes from Assembled Units of the Generated Model: Rigid Geometry with Rotation about One Diagonal/Axis	208

Fig. 5.10	Doubly Curved Folded Surface Generated Using Rigid Geometry Approach with Rotation about Both Diagonals	210
Fig. 5.11	Rendered Views of the Generated Model: Rigid Geometry with Rotation about Both Diagonals	211
Fig. 5.12	Shapes Assembled Using Two and Three Units of the Generated Model: Rigid Geometry with Rotation about Both Diagonals	212
Fig. 5.13	Shapes Assembled Using Four and Five Units of the Generated Model: Rigid Geometry with Rotation about Both Diagonals	213
Fig. 5.14	Image of *J. altifrons* Leaf (C) with Fringe Projection	215
Fig. 5.15	Meshed and Rendered Shapes of Leaf (C)	215
Fig. 5.16	Step 1- Forming Curved Edges Based on Model Obtained from Structured Lighting Method: Natural Geometry Approach	216
Fig. 5.17	Step 2 – Meshing the Right Half of the Leaf: Natural Geometry Approach	216
Fig. 5.18	Step 3 – Generation of Identical Surface through Shifting: Natural Geometry Approach	217
Fig. 5.19	Step 4 – Generation of Zigzag Boundary: Natural Geometry Approach	217
Fig. 5.20	Step 5 – Generation of Folds: Natural Geometry Approach	218
Fig. 5.21	3D Mesh of the Left Half of the Leaf - Modeled Separately: Natural Geometry Approach	218
Fig. 5.22	Rendered Shapes of Both Sides of the Leaf Model: Natural Geometry Approach	219
Fig. 5.23	Meshed and Rendered Shapes of the Generated Leaf Model after Assembling the Two Sides: Natural Geometry Approach	220
Fig. 5.24	Hyperbolic Parabloid Folded Surface with Folds Running in One Direction	222
Fig. 5.25	Assembly of Three Units of Hyperbolic Parabloid Folded Surface	223
Fig. 5.26	Folded Conoid	224
Fig. 5.27	Assembly of Six Units of Folded Conoid	225
Fig. 6.1	Meshed Model of Surface Data of Leaf (A)	230
Fig. 6.2	Meshed Model of Surface Data of Leaf (B)	231
Fig. 6.3	Top Edge of Leaf (A) before and after Smoothening	232
Fig. 6.4	Top Edge of Leaf (B) before and after Smoothening	232
Fig. 6.5	Bottom Parts of Leaf (A) and Leaf (B) Modeled Using Finer Mesh	233
Fig. 6.6	Typical Diagram for Geometrical Modeling of the Stem Line	235

Fig. 6.7	Bridging the Gap between Modeled Stem Line and Edge of Folded Leaf Surface Using Transition Zone Meshing	237
Fig. 6.8	Final Representative Typical Leaf Model	238
Fig. 6.9	Finite Element Geometrical Model of Leaf (A)	239
Fig. 6.10	Finite Element Geometrical Model of Leaf (B)	240
Fig. 6.11	Generation of Flattened Surfaces from Folded Versions	242
Fig. 6.12	Full Versions of Folded and Flattened Models of Leaf (A), Merged Together	243
Fig. 6.13	Full Versions of Folded and Flattened Models of Leaf (B), Merged Together	244
Fig. 6.14	Meshed and Rendered Models of Flattened Version of Leaf (A)	245
Fig. 6.15	Meshed and Rendered Models of Flattened Version of Leaf (B)	246
Fig. 6.16	Olympus BX50 Microscope Fitted with Colour Video Camera Used in Imaging the Stem Cross-Sections	248
Fig. 6.17	Cut Sections along the Stem of Leaf (A)	249-250
Fig. 6.18	Cut Sections along the Stem of Leaf (B)	251-252
Fig. 6.19	Sample of MIDAS/SPC Interface and Output for Section Properties Calculation (Section 1 – Leaf (A))	255
Fig. 6.20	Variation of Section Properties along the Stems of Leaves (A) and (B)	257-259
Fig. 6.21	Sample Picture Used for Thickness Measurement	260
Fig. 6.22	Density Plot of Samples Taken along Stems of Leaves (A) and (B)	261
Fig. 6.23(a)	Specimen Image for Area Measurement of Leaf Surface	262
Fig. 6.23(b)	Specimen Image for Thickness Measurement of Leaf Surface	262
Fig. 6.24	Average Density of the Folded Surface – Leaves (A) and (B)	263
Fig. 6.25	Thickness Variation of the Folded Surface – Leaves (A) and (B)	263
Fig. 6.26	Sign Convention for ECS and Element Forces (or Stresses) of a Beam Element	267
Fig. 6.27	Arrangement of Plate Elements and their ECS	269
Fig. 6.28	Sign Convention for Nodal Forces at Each Node of Plate Elements	270
Fig. 6.29	Output of Plate Element Forces, Stresses and Sign Convention	271
Fig. 6.30	Three Principal Axes of Wood with Respect to Grain Direction and Growth Rings	273

Fig. 6.31	Performance of the Transition Zone, Displacement along Fringe Line 11 – Leaf (A)	279
Fig. 6.32	Performance of the Transition Zone, Displacement along Fringe Line 38 – Leaf (A)	280
Fig. 6.33	Performance of the Transition Zone, Displacement along Fringe Line 59 – Leaf (A)	281
Fig. 6.34	Diagram Showing the Nodes Considered for Performance Evaluation of the Transition Zone	282
Fig. 6.35	Leaf (A) Model before and after Reorientation	285
Fig. 6.36(a)	Grouping of Elements for Thickness Assignment on the Surface of Leaf (A)	287
Fig. 6.36(b)	Grouping of Elements for Surface Thickness Assignment at the Bottom of Leaf (A)	288
Fig. 6.37(a)	Stem Axial Force (Fx), Leaf (A) - Folded and Flattened Models	296
Fig. 6.37(b)	Stem Shear Force (Fy), Leaf (A) - Folded and Flattened Models	296
Fig. 6.37(c)	Stem Shear Force (Fz), Leaf (A) - Folded and Flattened Models	297
Fig. 6.37(d)	Stem Torsional Moment (Mx), Leaf (A) - Folded and Flattened Models	297
Fig. 6.37(e)	Stem Bending Moment (My), Leaf (A) - Folded and Flattened Models	298
Fig. 6.37(f)	Stem Bending Moment (Mz), Leaf (A) - Folded and Flattened Models	298
Fig. 6.37(g)	Stem Axial Stress (Sax), Leaf (A) - Folded and Flattened Models	299
Fig. 6.37(h)	Stem Shear Stress (Ssy), Leaf (A) - Folded and Flattened Models	299
Fig. 6.37(i)	Stem Shear Stress (Ssz), Leaf (A) - Folded and Flattened Models	300
Fig. 6.37(j)	Stem Bending Stress (Sby), Leaf (A) - Folded and Flattened Models	300
Fig. 6.37(k)	Stem Bending Stress (Sbz), Leaf (A) - Folded and Flattened Models	301
Fig. 6.37(l)	Stem Combined Stresses (Sax, ±Sby and ±Sbz), Leaf (A) - Folded and Flattened Models	301
Fig. 6.37(m)	Superimposed Stem Stresses (Sax, ±Sby & ±Sbz and Combined Stress), Leaf (A) - Folded Model	302
Fig. 6.38	Leaf (B) Model before and after Reorientation	304
Fig. 6.39(a)	Grouping of Elements for Thickness Assignment on the Surface of Leaf (B)	306

Fig. 6.39(b)	Grouping of Elements for Surface Thickness Assignment at the Bottom of Leaf (B)	307
Fig. 6.40(a)	Stem Axial Force (Fx), Leaf (B) - Folded and Flattened Models	315
Fig. 6.40(b)	Stem Shear Force (Fy), Leaf (B) - Folded and Flattened Models	315
Fig. 6.40(c)	Stem Shear Force (Fz), Leaf (B) - Folded and Flattened Models	316
Fig. 6.40(d)	Stem Torsional Moment (Mx), Leaf (B) - Folded and Flattened Models	316
Fig. 6.40(e)	Stem Bending Moment (My), Leaf (B) - Folded and Flattened Models	317
Fig. 6.40(f)	Stem Bending Moment (Mz), Leaf (B) - Folded and Flattened Models	317
Fig. 6.40(g)	Stem Axial Stress (Sax), Leaf (B) - Folded and Flattened Models	318
Fig. 6.40(h)	Stem Shear Stress (Ssy), Leaf (B) - Folded and Flattened Models	318
Fig. 6.40(i)	Stem Shear Stress (Ssz), Leaf (B) - Folded and Flattened Models	319
Fig. 6.40(j)	Stem Bending Stress (Sby), Leaf (B) - Folded and Flattened Models	319
Fig. 6.40(k)	Stem Bending Stress (Sbz), Leaf (B) - Folded and Flattened Models	320
Fig. 6.40(l)	Stem Combined Stress (Sax, ±Sby and ±Sbz), Leaf (B) – Folded and Flattened Models	320
Fig. 6.40(m)	Superimposed Stem Stresses (Sax, ±Sby, ±Sbz and Combined Stress), Leaf (B) - Folded Model	321
Fig. 7.1(a)	10x Scaled-up Flattened Model	343
Fig. 7.1(b)	10x Scaled-up 10 Folds Model	343
Fig. 7.1(c)	10x Scaled-up 8 Folds Model	343
Fig. 7.1(d)	10x Scaled-up 6 Folds Model	343
Fig. 7.1(e)	10x Scaled-up 4 Folds Model	343
Fig. 7.2	Steps of Overcoming the Gap Problem between the Coons Mesh and the Natural Leaf Mesh	344
Fig. 7.3	Typical Diagram Showing Common Dimensions of All Practical Models Inspired from the *J. altifrons*	346
Fig. 7.4	Front and Rear Views of the 10x Scaled-Up 4 Folds Model	348
Fig. 7.5	Front and Rear Views of the 10x Scaled Up-6 Folds Model	349
Fig. 7.6	Labeling of Leaf-Like Model Parts for Stress Discussion Purpose	357
Fig. A1	Arrangement of Folded and Flat Plates of Equal Width	378
Fig. A2	Detailed Diagram of Unit Folded Plate	378

Fig. A3	Plot of ($I_{x' \text{ folded plate}}$ / $I_{x' \text{ flat plate}}$) Ratio versus Section Depth	380
Fig. B1	Camera Image Geometry	381
Fig. C1	Geometry of Proposed Approach	384
Fig. C2	Projector Dimensions	385
Fig. C3	Kodak Ektalite 500 Chart for Focal Length Calculation	386
Fig. C4	Horizontal Setup of Projector	386
Fig. C5	Projector Setup at an Inclined Angle θ	387
Fig. I1	Deformed Shape, Leaf (A) - Folded Model	403
Fig. I2	Displacement Contour, Leaf (A) - Folded Model	403
Fig. I3	Plate Axial Force (Fxx), Leaf (A) - Folded Model	404
Fig. I4	Plate Axial Force (Fyy), Leaf (A) - Folded Model	404
Fig. I5	Plate In-Plane Shear Force (Fxy), Leaf (A) - Folded Model	405
Fig. I6	Plate Bending Moment (Mxx), Leaf (A) - Folded Model	405
Fig. I7	Plate Bending Moment (Myy), Leaf (A) - Folded Model	406
Fig. I8	Plate Torsional Moment (Mxy), Leaf (A) - Folded Model	406
Fig. I9	Plate Axial Stress (σ_x) at Top, Leaf (A) - Folded Model	407
Fig. I10	Plate Axial Stress (σ_x) at Bottom, Leaf (A) - Folded Model	407
Fig. I11	Plate Axial Stress (σ_y) at Top, Leaf (A) - Folded Model	408
Fig. I12	Plate Axial Stress (σ_y) at Bottom, Leaf (A) - Folded Model	408
Fig. I13	Plate In-Plane Shear Stress (σ_{xy}) at Top, Leaf (A) – Folded Model	409
Fig. I14	Plate In-Plane Shear Stress (σ_{xy}) at Bottom, Leaf (A) – Folded Model	409
Fig. J1	Deformed Shape, Leaf (A) - Flattened Model	410
Fig. J2	Displacement Contour, Leaf (A) - Flattened Model	410
Fig. J3	Plate Axial Force (Fxx), Leaf (A) - Flattened Model	411
Fig. J4	Plate Axial Force (Fyy), Leaf (A) - Flattened Model	411
Fig. J5	Plate In-Plane Shear Force (Fxy), Leaf (A) – Flattened Model	412
Fig. J6	Plate Bending Moment (Mxx), Leaf (A) - Flattened Model	412
Fig. J7	Plate Bending Moment (Myy), Leaf (A) - Flattened Model	413
Fig. J8	Plate Torsional Moment (Mxy), Leaf (A) - Flattened Model	413
Fig. J9	Plate Axial Stress (σ_x) at Top, Leaf (A) - Flattened Model	414
Fig. J10	Plate Axial Stress (σ_x) at Bottom, Leaf (A) – Flattened Model	414
Fig. J11	Plate Axial Stress (σ_y) at Top, Leaf (A) - Flattened Model	415
Fig. J12	Plate Axial Stress (σ_y) at Bottom, Leaf (A) – Flattened Model	415

Fig. J13	Plate In-Plane Shear Stress (σ_{xy}) at Top, Leaf (A) – Flattened Model	416
Fig. J14	Plate In-Plane Shear Stress (σ_{xy}) at Bottom, Leaf (A) – Flattened Model	416
Fig. K1	Deformed Shape, Leaf (B) - Folded Model	417
Fig. K2	Displacement Contour, Leaf (B) - Folded Model	417
Fig. K3	Plate Axial Force (Fxx), Leaf (B) - Folded Model	418
Fig. K4	Plate Axial Force (Fyy), Leaf (B) - Folded Model	418
Fig. K5	Plate In-Plane Shear Force (Fxy), Leaf (B) - Folded Model	419
Fig. K6	Plate Bending Moment (Mxx), Leaf (B) - Folded Model	419
Fig. K7	Plate Moment Bending (Myy), Leaf (B) - Folded Model	420
Fig. K8	Plate Torsional Moment (Mxy), Leaf (B) - Folded Model	420
Fig. K9	Plate Axial Stress (σ_x) at Top, Leaf (B) - Folded Model	421
Fig. K10	Plate Axial Stress (σ_x) at Bottom, Leaf (B) - Folded Model	421
Fig. K11	Plate Axial Stress (σ_y) at Top, Leaf (B) - Folded Model	422
Fig. K12	Plate Axial Stress (σ_y) at Bottom, Leaf (B) - Folded Model	422
Fig. K13	Plate In-Plane Shear Stress (σ_{xy}) at Top, Leaf (B) – Folded Model	423
Fig. K14	Plate In-Plane Shear Stress (σ_{xy}) at Bottom, Leaf (B) – Folded Model	423
Fig. L1	Deformed Shape, Leaf (B) - Flattened Model	424
Fig. L2	Displacement Contour, Leaf (B) - Flattened Model	424
Fig. L3	Plate Axial Force (Fxx), Leaf (B) - Flattened Model	425
Fig. L4	Plate Axial Force (Fyy), Leaf (B) - Flattened Model	425
Fig. L5	Plate In-Plane Shear Force (Fxy), Leaf (B) – Flattened Model	426
Fig. L6	Plate Bending Moment (Mxx), Leaf (B) - Flattened Model	426
Fig. L7	Plate Bending Moment (Myy), Leaf (B) - Flattened Model	427
Fig. L8	Plate Torsional Moment (Mxy), Leaf (B) - Flattened Model	427
Fig. L9	Plate Axial Stress (σ_x) at Top, Leaf (B) - Flattened Model	428
Fig. L10	Plate Axial Stress (σ_x) at Bottom, Leaf (B) – Flattened Model	428
Fig. L11	Plate Axial Stress (σ_y) at Top, Leaf (B) - Flattened Model	429
Fig. L12	Plate Axial Stress (σ_y) at Bottom, Leaf (B) – Flattened Model	429
Fig. L13	Plate In-Plane Shear Stress (σ_{xy}) at Top, Leaf (B) – Flattened Model	430
Fig. L14	Plate In-Plane Shear Stress (σ_{xy}) at Bottom, Leaf (B) – Flattened Model	430

Fig. M1	Deformed Shape - 4 Folds Models	431
Fig. M2	Displacement Contour - 4 Folds Models	432
Fig. M3	Displacement Contour of the Folded Surface - 4 Folds Models	433
Fig. M4	Displacement Contour of the Stem - 4 Folds Models	434
Fig. M5	Folded Plate Bending Moment (Mxx) - 4 Folds Models	435
Fig. M6	Folded Plate Bending Moment (Myy) - 4 Folds Models	436
Fig. M7	Folded Plate Torsional Moment (Mxy) - 4 Folds Models	437
Fig. M8	Folded Plate Axial Stress (σ_x) at Top - 4 Folds Models	438
Fig. M9	Stem Plate Axial Stress (σ_x) at Top - 4 Folds Models	439
Fig. M10	Folded Plate Axial Stress (σ_x) at Bottom - 4 Folds Models	440
Fig. M11	Stem Plate Axial Stress (σ_x) at Bottom - 4 Folds Models	441
Fig. M12	Folded Plate Axial Stress (σ_y) at Top - 4 Folds Models	442
Fig. M13	Stem Plate Axial Stress (σ_y) at Top - 4 Folds Models	443
Fig. M14	Folded Plate Axial Stress (σ_y) at Bottom - 4 Folds Models	444
Fig. M15	Stem Plate Axial Stress (σ_y) at Bottom - 4 Folds Models	445
Fig. M16	Folded Plate In-Plane Shear Stress (σ_{xy}) at Top - 4 Folds Models	446
Fig. M17	Stem Plate In-Plane Shear Stress (σ_{xy}) at Top - 4 Folds Models	447
Fig. M18	Folded Plate In-Plane Shear Stress (σ_{xy}) at Bottom – 4 Folds Models	448
Fig. M19	Stem Plate In-Plane Shear Stress (σ_{xy}) at Bottom - 4 Folds Models	449
Fig. N1	Deformed Shape - 6 Folds Models	450
Fig. N2	Displacement Contour - 6 Folds Models	451
Fig. N3	Displacement Contour of the Folded Surface - 6 Folds Models	452
Fig. N4	Displacement Contour of the Stem - 6 Folds Models	453
Fig. N5	Folded Plate Bending Moment (Mxx) - 6 Folds Models	454
Fig. N6	Folded Plate Bending Moment (Myy) - 6 Folds Models	455
Fig. N7	Folded Plate Torsional Moment (Mxy) - 6 Folds Models	456
Fig. N8	Folded Plate Axial Stress (σ_x) at Top - 6 Folds Models	457
Fig. N9	Stem Plate Axial Stress (σ_x) at Top - 6 Folds Models	458
Fig. N10	Folded Plate Axial Stress (σ_x) at Bottom - 6 Folds Models	459
Fig. N11	Stem Plate Axial Stress (σ_x) at Bottom - 6 Folds Models	460
Fig. N12	Folded Plate Axial Stress (σ_y) at Top - 6 Folds Models	461
Fig. N13	Stem Plate Axial Stress (σ_y) at Top - 6 Folds Models	462

Fig. N14	Folded Plate Axial Stress (σ_y) at Bottom - 6 Folds Models	463
Fig. N15	Stem Plate Axial Stress (σ_y) at Bottom - 6 Folds Models	464
Fig. N16	Folded Plate In-Plane Shear Stress (σ_{xy}) at Top - 6 Folds Models	465
Fig. N17	Stem Plate In-Plane Shear Stress (σ_{xy}) at Top - 6 Folds Models	466
Fig. N18	Folded Plate In-Plane Shear Stress (σ_{xy}) at Bottom – 6 Folds Models	467
Fig. N19	Stem Plate In-Plane Shear Stress (σ_{xy}) at Bottom - 6 Folds Models	468

LIST OF ABBREVIATION

ACI	American Concrete Institute
ASCE	American Society of Civil Engineers
BIONIS	The Biomimetics Network for Industrial Sustainability
CBNT	Centre for Biomimetics and Natural Technologies
CBUR	Centre for Biomimetics, University of Reading
CITES	Convention on International Trade in Endangered Species of Wild Flora and Fauna
DNA	Deoxyribonucleic acid
ECS	Element Coordinate System
EERC	Earthquake Engineering Research Center
ESA	European Space Agency
FEA	Finite Element Analysis
FSDT	First Order Shear Deformation Theory
GCS	Global Coordinate System
J. altifrons	*Johannesteijsmannia altifrons*
MSU	Michigan State University
MWOD	Merriam-Webster Online Dictionary
MZUM	Museum of Zoology, University of Michigan
NRCS	Natural Resources Conservation Service
PACSOF	Palm and Cycad Societies of Florida, Inc.
PSSDB	Profiled Steel Sheeting/Dry Board
RE	Reverse Engineering
SDUD	Senate Department of Urban Development
SPC	Sectional Property Calculator
SRC	Source Referenced Classification
TPT	Two Point Triangulation
TRIZ	Russian acronym for (Teoriya Resheniya Izobretatelskikh Zadatch) i.e. Theory of Inventive Problem Solving
TWA	Trans World Airlines

LIST OF SYMBOLS

A_{sy}	Effective Shear Area for shear force in the element's local y-direction
A_{sz}	Effective Shear Area for shear force in the element's local z-direction
C_{ym}	Distance from the section's neutral axis to the extreme fiber of the element in the local (-)y-direction
C_{yp}	Distance from the section's neutral axis to the extreme fiber of the element in the local (+)y-direction
C_{zm}	Distance from the section's neutral axis to the extreme fiber of the element in the local (-)z-direction
C_{zp}	Distance from the section's neutral axis to the extreme fiber of the element in the local (+)z-direction
Combined	Combined beam stress (Combined stress: Maximum or minimum value among Sax ± Sby ± Sbz)
E	Modulus of elasticity (GPa)
E_L (E_x)	Modulus of elasticity in the longitudinal direction of wood
E_R (E_Z)	Modulus of elasticity in the radial direction of wood
E_T (E_y)	Modulus of elasticity in the tangential direction of wood
f_c	Characteristic compressive strength of concrete (MPa)
Fx	Axial force in the beam element's local x-direction
Fxx	Axial force per unit width in the plate element's local or GCS x-direction (Perpendicular to local yz-plane)
Fxy	Shear force per unit width in the plate element's local or GCS xy-direction (In-plane shear)
Fy	Shear force in the beam element's local y-direction
Fyy	Axial force per unit width in the plate element's local or GCS y-direction (Perpendicular to local xz-plane)
Fz	Shear force in the beam element's local z-direction
G	Shear modulus of (MPa)
G_{LR} (G_{xz})	Modulus of rigidity in the LR (xz) plane of wood
G_{LT} (G_{xy})	Modulus of rigidity in the LT (xy) plane of wood
G_{TR} (G_{yz})	Modulus of rigidity in the TR (yz) plane of wood
I_{xx}	Torsional Resistance about the element's local x-axis, or the J value
I_{yy}	Moment of Inertia about the element's local y-direction
I_{zz}	Moment of Inertia about the element's local z-direction
L or x	Longitudinal axis parallel to the fiber or grain of wood
Mx	Torsional moment about the beam element's local x-axis
Mxx	Bending moment per unit width in the direction of the plate element's local or GCS x-axis (Out-of-plane moment about local y-axis)

Mxy	Torsional moment per unit width about the plate element's local or GCS xy-plane
My	Bending moment about the beam element's local y-axis
Myy	Bending moment per unit width in the direction of the plate element's local or GCS y-axis (Out-of-plane moment about local x-axis)
Mz	Bending moment about the beam element's local z-axis
Peri-O	Total perimeter of the section
Peri-I	Inside perimeter length of a hollow section
R or z	Radial axis normal to the growth rings of wood
Q_{yb}	Shear Coefficient for the shear force applied in the element's local z-direction
Q_{zb}	Shear Coefficient for the shear force applied in the element's local y-direction
Sax	Axial stress in the beam element's local x-direction
Sig-xx (σ_x)	Axial stress in the plate element's local x-direction (Perpendicular to local yz-plane)
Sby	Bending stress about the beam element's local y-axis
Sbz	Bending stress about the beam element's local z-axis
Ssy	Shear stress in the beam element's local y-direction
Ssz	Shear stress in the beam element's local z-direction
Sig-yy (σ_y)	Axial stress in the plate element's local y-direction (Perpendicular to local xz-plane)
Sig–xy (σ_{xy})	Shear stress in the plate element's local xy-plane (In-plane shear stress)
T or y	Tangential axis to the growth ring of wood
μ_{LT} (μ_{xy})	Poisson’s ratio for deformation along the tangential axis caused by stress along the longitudinal axis
μ_{LR} (μ_{xz})	Poisson’s ratio for deformation along the radial axis caused by stress along the longitudinal axis
μ_{TR} (μ_{yz})	Poisson’s ratio for deformation along the radial axis caused by stress along the tangential axis
μ	Poisson’s ratio

SATU KAJIAN ANALISIS TENTANG BENTUK STRUKTUR KELOMPANG BERLENGKUNGAN KEMBAR BERLIPAT BARU YANG DIILHAMKAN ALAM SEMULAJADI

ABSTRAK

Kajian ini mengenai daun dari tumbuhan *Johannesteijsmannia altifrons* (*J. altifrons*) yang tergolong dalam keluarga palma telah diselidik. Daun *J.altifrons* menyerupai struktur kelompang terjulur berkelengkungan kembar dengan lipatan yang berunjur dari anggota tunjang tengah. Tujuan penyelidikan ini dijalankan dengan mensasarkan dua perkara berikut : untuk mengkaji pengaruh bentuk dan lipatan keatas kelakuan struktur *J.altifrons* dan untuk menyiasat kelakuan model struktur dengan saiz sebenar mirip *J.altifrons* yang memenuhi keperluan praktikal menggunakan kaedah elemen terhingga. Satu kaedah tanpa-sentuh yang dikenali sebagai kaedah pencahayaan berstruktur telah digunakan untuk mendapatkan data permukaan daun yang dikaji. Satu algoritma yang berdasarkan geometri sebenar pemasangan pengukuran dengan tujuan untuk mengurangkan masalah paralaks telah dibangunkan dan digunakan dalam kajian ini. Kelakuan struktur model analisis yang dijana berdasarkan bentuk daun yang dipilih telah diselidik dengan menggunakan kaedah elemen terhingga. Model analisis yang berkenaan telah dianalisa dengan menggunakan sebelas jenis spesis kayu. Keputusan analisis menunjukkan prestasi struktur yang cekap dari segi kekukuhan dan kekuatan. Untuk tujuan menyelidik kesan lipatan keatas kelakuan struktur, permukaan melengkung tanpa lipatan, yang mempunyai bentuk permukaan yang serupa dengan daun kajian, telah dijana dan dianalisa. Model analisis dengan lipatan menunjukkan prestasi dari segi kekukuhan dan kekuatan yang lebih baik berbanding dengan model analisis tanpa lipatan. Model analisis dengan lipatan yang mempunyai bentuk melengkung “synclastic” dan “anticlastic” menghasilkan anjakan maksima sebanyak lebih kurang 70% dan 30% daripada nilai anjakan maksima model analisis tanpa lipatan. Perbandingan dalam magnitud tegasan tegangan dan mampatan memberikan nilai lebih kurang 40% dan

20% daripada tegasan dalam model analisis tanpa lipatan. Memandangkan sifat penyelidikan ini yang melibatkan bidang “biomimetic”, satu kaedah yang mudah yang diberi nama sebagai “Source Reference Classification” (SRC) untuk tujuan pengkelasan pencapaian dalam bidang teknologi yang diilhamkan oleh alam semulajadi juga telah diperkenalkan. Satu prosedur baru yang berdasarkan CAD juga telah dibangunkan untuk tujuan penjanaan permukaan melengkung dengan lengkungan kembar yang berlipat. Satu kajian pengiraan berkomputer telah dijalankan keatas model yang dijana untuk menilai prestasi struktur mereka dibawah keadaan beban berat sendiri dengan menggunakan bahan konkrit ringan. Keputusan analisis menunjukkan prestasi struktur yang memuaskan dari segi kekukuhan dan kekuatan dengan keupayaan simpanan bahan yang sangat besar terutamanya dalam menanggung tegasan mampatan (lebih kurang 88%). Kesemua 6 model menunjukkan anjakan maksima kurang daripada 15 mm berbanding dengan rentang julur lebih kurang 10 m.

A COMPUTATIONAL STUDY ON A NATURE INSPIRED NOVEL DOUBLY CURVED FOLDED SHELL STRUCTURAL FORM

ABSTRACT

In this research, the leaves of *Johannesteijsmannia altifrons* (*J. altifrons*) which belong to the palm family have been investigated. These leaves are doubly curved cantilever shell structures with folds extending from the central spine. The target of the study is in two folds: to investigate the influence of shape and folds on the structural behaviour of the *J. altifrons* and to investigate the structural behaviour of the *J. altifrons* like scaled-up, realistic models under practical considerations using finite element analysis. A non-contact method called *structured lighting method* has been used for capturing the surface data of the leaf. An algorithm based on the actual geometry of the imaging setup has been developed and used in this study. The leaves have been analysed using orthotropic material properties of eleven species of wood. The results show efficient structural performance of the leaves in terms of stiffness and strength. In order to study the influence of the folds on structural behaviour, non-folded versions have also been generated and analysed. Folded models showed better performance in terms of stiffness and strength compared to the non-folded versions. The synclastic and anticlastic folded models yielded maximum deflection values of about 70% and 30% of the values in the corresponding flattened models, respectively. Similar comparison in terms of stresses yielded values of about 40% and 20% of the corresponding stresses in flattened models for both tension and compression. In view of the biomimetic nature of the study, a simple method called *Source Referenced Classification* (SRC) to classify nature inspired technological achievements is also presented. Novel CAD based procedures have also been developed for the purpose of generating doubly curved surfaces with folds. These procedures have been implemented to generate leaf-like scaled-up models. A computational study is carried out on these models to evaluate their structural performance under self weight condition, using light weight concrete. The results show satisfactory performance in

terms of stiffness and strength with considerable reserve in material capacity particularly in compression (about 88%). All 6 models showed maximum deflection values of less than 15 mm over cantilever spans of about 10 m.

CHAPTER 1
INTRODUCTION

1.1 General

Shells are surfaces with high structural performance in terms of self-weight to load carrying capacity. Such a characteristic combined with the inherent stiffness and beauty always qualifies shells for special engineering applications where architectural beauty and coverage of large continuous spaces are the main functional requirements. Xochimilco Restaurant (Mexico City, Mexico 1958), TWA Terminal at JFK Airport (New York, USA 1962), Sydney Opera House (Sydney, Australia 1973), Aquatic Centre (Baden Württemberg, Germany 1987) and Putrajaya Convention Centre (Putrajaya, Malaysia 2003) are among the famous successful applications (Fig. 1.1). Over the last few decades, advancements in the structural analysis domain and computational tools enabled engineers to satisfactorily analyze and build shells of different complicated types and forms. On the contrary, shells with very wide variety of shapes and breathtaking elegance existed in nature since millions of years.

Surfaces found in nature offer a rich source of ideas for possible applications as engineering structures. Animal shells, sea shells and plant leaves are among the natural surfaces that serve as potential sources of mimicry for new structural systems. Nature is very smart in optimizing shape and material; comprehensive understanding of how nature handles such tasks under tight environmental constraints that are limited as well as unfavourable is a key issue to many researchers today. Using ideas from nature is justifiable based on the fact that existing natural systems could survive over thousands of years through adapting to the prevailing environmental conditions using nature's limited resources in an amazingly efficient manner. In case of engineering structures and materials the concern is cash cost whereas in case of natural systems, the cost is energy and the competition is not commercial but the more severe one of nature where the fittest survive and failures remain as fossils.

(a) Xochimilco Restaurant, Mexico

(b)TWA Terminal at JFK Airport, New York

(c) Opera House, Sydney

(d) Aquatic Centre, Baden Württemberg

(e) Convention Centre, Putrajaya

Fig. 1.1: Some Successful Shell Applications (http://en.structurae.de/structures/stype/index.cfm?ID=1009 – Accessed 24th June 2007)

1.2 Background of the Study

A closer look at the features of engineered or man-made structures and structures in nature reveal striking similarities. Despite the fact that natural systems operate with different scales, functions and processes, 'the design constraints' and 'the objectives' remain similar to what humans create. Functionality, optimization and cost effectiveness are the main concern of engineering design. Likewise a minimized blend of material and energy consumption is the working principle of natural systems. As such, efficient, light and rigid structures in nature exhibiting high capacity to withstand internal and external forces in an optimum manner have always been a source of inspiration for many architects and engineers (Arslan and Sorguc, 2004). Nature inspired structures have been categorized into five groups based on their 'animate' and 'inanimate' nature. These groups are: tree-like structures, web-like structures, shell-like structures, skeleton-like structures and pneumatic structures (Arslan and Sorguc, 2004).

Despite the uncertainty whether some remarkable engineering structures were inspired from nature or not, yet their counterparts in nature with striking similarities have been identified as can be observed from the examples described in the following paragraphs.

A tensegrity structure is an assembly of rigid and flexible members called struts and cables/strings forming compression and tension members, respectively. They may also comprise rigid members only, carrying compression and tension forces. Equilibrium of tensegrity structures is a function of the relative arrangement of the compression and tension members that results in balanced distribution of the mechanical stresses. They fall under two categories including the geodesic domes (the Buckminster Fuller domes) and structures that attain stability through prestressing (sculptures of Kenneth Snelson) (Ingber, 1998). The design concept of the geodesic dome of Buckminster Fuller looks like the structure of an insect's eye. The natural eye shape of the insect is a hemisphere containing several parts that are held together and

supported by a natural geodesic dome grid on the outside surface. The hemispherical grid serves as a strong interconnected structural framework providing a stiff support for the cornea (Gildea, 1998). Ingber (1998) stated that the principle of tensegrity can be observed at all detectable scales of the human body. Muscles, tendons and ligaments are the tension members which balance the 206 bones representing the compression members. At the micro level cells, proteins and molecules also stabilize themselves through the principle of tensegrity.

Meadows (1999) wrote on the probable idea behind the design of the Crystal Palace which seems to be inspired from the giant leaves of *Victoria amazonica* (the water lily). Joseph Paxton, inspired by the water lily, built a greenhouse with a roof structure similar to that of the leaf's ribbed surface. A further step to this was the Crystal Palace (London) that was 108 ft high, covering an area of 18 acres. The building was completed in 1851 and collapsed under fire in 1936. On the contrary, Vincent *et al*. (2006) argued that the corrugated structure of the Crystal Palace resembles more other types of leaves, such as beech or hornbeam, than the tapering beam-like structure of the water lily.

The structure of the trabecular struts in the head of the human femur or the tapered form of the tulip stem appear to have inspired the design of Paris' landmark, the Eiffel's tower (Vincent *et al*., 2006). Hermann Von Meyer, professor of anatomy at Zurich observed that the femur head looks like a group of bones arranged in a curved path. Karl Cullman, a Swedish engineer, understood such a bone structure as paths along which the stresses, induced by the eccentric hip forces, are transferred to the bones of the leg. The French engineer, Gustaff Eiffel, implemented the idea in the design of the tower where four inverted femur-like components were employed to transfer the tower's load to the foundation (Rao, 2003).

In the context of this study, nature inspired structures are referred to as: structures inspired from non-biological systems and those inspired from biological systems. Structures inspired from natural physical phenomena such as the soap film,

sagging strings/ropes and inverted hanging fabrics fall under the former category. On the other hand, structures inspired from human body, animals and plants belong to the latter category. A review with some examples belonging to each category is presented in the following two sections.

1.2.1 Structures Inspired from Non-Biological Systems

The soap film, the natural catenary shapes of hanging chains/ropes and the hanging reversed membranes are among the natural physical forms that inspired the design of many engineering structures of the twentieth century.

From 1965 to 1991 Frei Otto and his interdisciplinary team of architects, biologists and engineers carried out studies on structures working on light weight principles. Among the structures investigated were those modeled after the “soap film” for tension membranes (Lewis, 2005). Soap films are minimal surfaces exhibiting proportionality of the energy of surface tension to the area of the surface. This illustrates a beautiful example in nature where the principle of minimum energy consumption is highlighted in the minimized area of the soap film (Jacobs, 2003). The most important requirement in the design of minimal surface membrane structure is the fulfillment of the equal stress criteria throughout the surface. Minimal surfaces can either be created using physical models or computer methods based on mathematical formulation. The Haj terminal at Jeddah International airport in Saudi Arabia is a minimal surface tension membrane structure (Bradshaw *et al*., 2002).

Antonio Gaudi (Spanish architect, 1852-1926) applied the approach of inverted hanging models in the design of his structures. He assembled models of hanging chains with small sand bags, serving as point loads. The original shape of the hanging chain was changed by the simulated point loads leading to naturally shaped “inverted” spires; a frozen inverted model reversed the force nature in the chains from tension to compression (Lewis, 2005).

The free form shells built by the famous Swiss engineer Heinz Isler (born 1926) were inspired from hanging models. Isler applied an experimental method to create a square-plan form through pouring a plastic material onto a cloth cover held at the corners and supported on a solid surface. When the fabric is evenly covered by the plastic material the wooden support was lowered allowing free flow formation of a natural physical shape in pure tension. Upside down turning of the solidified model gave a shell form in pure compression. Bürgi Garden Centre in Camorino, Grötzingen outdoor theatre near Stuttgart are examples of shells designed using the “flowing method” (Billington, 2003).

1.2.2 Structures Inspired from Biological Systems

Spider web, honeycomb and seashells are natural biological structures that illustrate efficient performance of natural creatures in blending shape and material, seeking adaptation during their survival journey.

Spiders fabricate webs that are resistant to water, rain and sunlight from barely visible fibers. Yet a spider fiber is estimated to be five times as strong as an equivalent steel wire (Benyus, 1997). Targeting adaptation, natural structures tend to employ tension members more efficiently than compression members that have the tendency to buckle. Such a feature can be observed in the spider web where maximum tension members are employed concentrating compression into localized zones. The web is fabricated with a network of tension strands; the spider and the captured prey act as localized compression struts. Frei Otto’s Olympic Stadium in Munich, Germany is a highly efficient tent structure inspired directly from the spider web (Johnson, 2003).

Honeycomb is a wax structure containing many hexagonal shaped cells built in complete darkness using minimum amount of material. It offers optimal packing shape and provides maximum space required to contain the honey and the larvae. Moreover, honeycomb structures are very useful panel stiffeners. Combination of these merits in one structure led to several applications such as the sandwich panels and the

construction of control surfaces of an aircraft where high strength, large dimensions and light weight are the main requirements. The internal hidden structure of elevators, aircraft wings, tail and many other parts comprise honeycomb structures (Bar-Cohen, 2006).

Seashells in nature occur in a variety of type, shape and colour. First traces in the long history of studies on seashells can be found in the work of Henry Moseley in 1838 (Jirapong and Krawczyk, 2003). Most of the work done on seashells focused on the mathematical aspects that control the overall geometry. A simple seashell may be represented as a surface generated through revolving a cross-section of constant shape along a spiral path about the shell axis. Different forms can be generated depending on the starting cross-section and the rate of change in its size. Based on this formulation, Jirapong and Krawczyk (2003) proposed a mathematical model to describe the spiral shell geometry with the objective of generating new architectural forms that can be used as input for structural analysis of the system. The model was integrated with CAD software that enables generation of new architectural forms (mesh models) through merely changing the model parameters.

1.3 Inspiring Source from Plants in Nature

Plants in nature with countless number of shapes and sizes offer a rich source of ideas for engineers. Leaves are cantilever shell-like structures whereas stems and branches are cellular or tubular structures that act as supporting members. The main stem can be thought of as a column member and the branches as cantilever beams that support the leaves.

Unlike the regular and conventional shapes of many man-made structural members, plant leaves show more complex shapes through folding, curling and rolling. They respond to the applied loads such as wind loads by changing shape thereby gaining structural stiffness without adding extra mass. King and Vincent (1996) carried out a study on a number of *Phormium* genotypes to calculate the stiffness with different

curl angles using CAD software. They concluded that gain in the structural stiffness of plants' leaf is a function of the leaf curling along and/or folding about the midrib. The study did not reveal any correlation between size of the keel (midrib) or thickness of leaf and stiffness.

Kobayashi *et al*. (1998) modeled the leaves of hornbeam and beach as plane surfaces, with straight parallel folds, using numerical methods and studied their folding patterns for applications to areas such as solar panels, light weight antennae for satellites, deployable membranes such as tents, clothes or other coverings.

Balz and Güring (2001) modeled the petal shapes of orchid blossom to study the shape-stability behaviour. They argue that blossoms are minimal constructions comprising 2% cellulose and 98% water. The double curved surface helps blossoms to attain stability in space. Stiffness is achieved from the inner cellular pressure and the double curved shell structure. They proposed this kind of structure for deployable or temporary buildings made of membranes and erected by air or water pressure.

De Focatiis and Guest (2002) looked into the deployment of tree leaves to find patterns for folding membranes aiming to arrive at structure which can be reduced in size for transportation or storage, and then automatically deployed.

Stuttgart airport terminal 3 in Germany is a modern engineering structure inspired from the world of plants; it very much resembles the stem and branches of a tree. The structure comprises 18 'steel tree' strut construction that carries the enormous mono-pitch roof. Each steel tree takes the form of a big circular steel section with several smaller sections branching at different levels to make an overall diameter of 18m at 15m height (PERI, 2006).

1.4 The *Johannesteijsmannia altifrons*

Shells in nature occur in a variety of sizes and shapes; of special interest to this study are the shell-like surfaces with folds which can be observed in leaves of many plants. This thesis investigates the structural behaviour of doubly curved folded

surfaces inspired from a magnificent palm leaf called the *Johannesteijsmannia altifrons* (*J. altifrons*) for possible application as novel engineering structures. The leaves of *J. altifrons* resemble a cantilevered shell structure with folds extending from the central spine. Such combination of shell surface and folds might have contributed to the ability of the leaves of *J. altifrons* to extend to a span of about 6 m. Apart from such positive characteristic, from the point of view of load carrying capacity, existence of folds has also added element of aesthetic to the natural surface due to the interplay of shadows caused by the folds. Folded surfaces form a special category of shell structures; a corrugated sheet has better structural performance than a plane sheet of the same material, thickness and coverage area. Existence of folds on the surface adds to its overall depth thereby enhancing the stiffness with respect to bending of the structure.

The inspiring source of this study, the magnificent leaf of *J. altifrons* belongs to the palm group (Fig. 1.2). In biological taxonomy it falls with other three species under the *Johannesteijsmannia* genus of forest palms. The other three species are *Johannesteijsmannia lanceolata, Johannesteijsmannia dransfield and Johannesteijsmannia perakensis*. They are native to southern Thailand, Peninsular Malaysia, Sumatra and western Borneo. The *J. altifrons* is the only species that is widely spread in southern Thailand, Peninsular Malaysia, western Sarawak, western Kalimantan and Sumatra. The other three species are mostly available in Peninsular Malaysia. The *J. altifrons* is also known as the “Joey Palm” or the “Diamond Joey” referring to its diamond-like shape. It is one of the most stunning and spectacular plants and the finest among the palm family. The habitat of the *J. altifrons* is the mountain rainforest slopes and ridge-tops that are about 500 m (1600 ft) high. Shady, wind protected subtropical and tropical regions are ideal for the Joey growth. It also shows good tolerance to cool climate. Shady location, abundant water, high humidity, warm temperature, well drained and rich soil that is slightly acidic are the favourable local conditions for the Joey growth and survival. The plant is very sensitive to root disturbance. When potting, removal of old soil and root trimming should be avoided as

these may lead to the plant death. Loss of habitat due to logging, deforestation, usage of the leaves for roof thatching and the seeds for export is threatening the existence of the four species. Lim and Whitmore (2000) reported that despite the widespread availability of the *J. altifrons* compared to the other species, it is considered under threat. Field observations over the last decade show a drastic drop in the *J. altifrons* population amounting to about quarter the original figure (Moore, 2003). In Sarawak, the Joey is totally protected and is also listed under CITES (Convention on International Trade in Endangered Species of Wild Flora and Fauna). The Joey leaves also resemble the crocodile tail; hence the local name “ekor buaya” (Chai, 1993).

Fig. 1.2: The Magnificent Palm – *Johannesteijsmannia altifrons*
(http://davesgarden.com/pf/showimage/23678/ - Accessed 24th June 2007)

The Joey is a medium size trunk-less palm with large diamond shaped undivided, leathery leaves that are about 3 m high when mature but, at times, may reach a height of about 6 m (Fig. 1.3). The giant leaves are characterized with serrated edges and approximately parallel pleats along their surface (Fig. 1.4). In engineering terms, the Joey looks like a cantilevered shell structure supported over the central spine. The leaf can be described as a rhomboid double curved or hyperbolic parabloid surface with nearly parallel folds extending throughout the leaf length. Combination of

these distinctive features qualifies the Joey as an ideal, highly competent natural shell illustrating striking performance in merging shape and material to enhance the load carrying capacity.

Fig. 1.3: Heights Reached by the *Johannesteijsmannia altifrons* (http://www.pacsoa.org.au/palms/Johannesteijsmannia/altifrons.html - Accessed 24th June 2007)

Fig. 1.4: Picture Showing Serrated Edge and Fold Lines on the *Johannesteijsmannia altifrons* (http://www.lundkvistpalmgarden.com/Johannesteijsmannia.html - Accessed 24th June 2007)

1.5 Problem Statement

As mentioned in the previous section, the magnificent leaves of *J. altifrons* reach a height of about 3 m when mature and sometimes extraordinary height of about 6 m. The shape/curvature and folds combination is likely to play a major role towards the structural behaviour of this natural system that has very small thickness relative to its surface area. Despite the modern technological advancements, such an efficient structural performance is generally difficult – yet not impossible - to achieve in man-made structures. Moreover, the existence of folds on the double curved surface of the *J. altifrons* gives a very pleasing appearance due to the interplay of shadows caused by the folds. Thus, the desired aspects of combining the structural efficiency and architectural beauty generally targeted in engineering structures are superbly displayed by the wonderful *J. altifrons*. As such, this study is carried out to investigate the geometry (shape and folds) influence towards the structural behaviour of the leaves. Comprehensive understanding of the structural behaviour of the leaves may lead to new structural forms that fulfill both the structural as well as the architectural requirements in terms of material usage and functionality. Moreover, this research work is the first to deal with doubly curved surfaces with folds; so far folded surfaces have been limited to flat and single curved shapes as will be seen in the literature review (Chapter 2).

1.6 Research Objectives

The focus of this research is to study the geometry (shape and folds) influence on the structural behaviour of the leaf of *J. altifrons* for possible engineering applications comprising double curved surfaces with folds. Therefore, the objectives are as follows:

i. To establish a modified algorithm based on the actual geometry of imaging setup for surface data acquisition of 3D objects derived from the conventional structured lighting method.
ii. To establish CAD based methods/procedures for modeling double curved surfaces with folds inspired from the leaf of *J. altifrons*.
iii. To investigate the influence of geometry on the structural behaviour of two units of *J. altifrons* leaves in their actual size and form. In this regard finite element analysis using orthotropic organic material (wood) is targeted.
iv. To investigate the structural behaviour of CAD generated, scaled-up, concrete models inspired from the *J. altifrons* preserving the actual double curved shape. Models with different number of folds are to be investigated using finite element analysis with the use of conventional construction material (concrete).

1.7 Scope of Research

This study is of interdisciplinary nature, it touches the disciplines of biomimicry, image-based measurements and structural engineering. The study subject (*J. altifrons*) is inspired from nature. The research focuses on the geometry (shape and folds) aspects of the leaf towards its structural behaviour; the actual leaf material is not considered in this study. The leaf shape is mimicked through optical/image based measurements using structured lighting method. Structural behaviour of two units of *J. altifrons* leaves is investigated under self weight condition using wood material and static analysis; analysis under imposed loads and dynamic conditions are not covered. Scaled up models inspired from the *J. altifrons*, for realistic applications, are generated using CAD based procedures that are developed during the course of this research. Static analysis is carried out under self weight conditions only using concrete material; imposed loads and dynamic analysis are not considered.

1.8 Thesis Layout

This thesis is complied in eight chapters. A brief outline of each chapter is given below:

- Chapter 1 describes the general overview and background of the research. A brief description of the study subject (*J. altifrons*) is also presented. This is, then, followed by the research objectives, problem statement, scope of research and the thesis layout.
- Chapter 2 presents the literature review on the subjects related to the research study. Shell and folded surfaces in nature and man-made folded structures are reviewed. Highlights on the research status and recent work on folded plate structures are also given.
- Chapter 3 introduces the idea of Source Referenced Classification (SRC) of the technological achievements inspired from biological systems. A method of cataloguing the different technological achievements inspired from nature is presented with illustrative examples.
- Chapter 4 deals with measurement aspects of the research subject. It presents the methodology followed in capturing the 3D surface data of the leaf of *J. altifrons*. Description of the conventional structured lighting method along with a modified version of the method to improve its outcome is introduced in this chapter. Verification of the proposed method is also carried out through measuring 3D objects of known dimensions. Measurement results and the 3D models of two units (Leaf (A) and Leaf (B)) of the *J. altifrons* are presented. These, represent the necessary input data to the finite element analysis of the leaves presented in Chapter 6.
- Chapter 5 presents CAD based procedures, developed during the course of the study, for generating double curved folded surfaces inspired from nature. It introduces stepwise CAD modeling procedures for generating doubly curved

folded surfaces with a variety of shapes. A procedure for generating leaf like surfaces with folds based on the natural leaf of *J. altifrons* is also presented. These procedures are applied to generate the models investigated in Chapter 7.

- Chapter 6 presents the finite element analysis aspects of Leaf (A) and Leaf (B). Necessary modeling aspects under finite element analysis software (MIDAS/Gen) of the stem and surface with regard to section properties, material, loading and support condition are illustrated. Results of the analysis of Leaf (A) and Leaf (B) are presented and discussed in this chapter.
- Chapter 7 consists of description on the generation of scaled-up versions inspired from Leaf (B) for realistic applications. Models with 4 and 6 folds, each in three different fold depths (10 cm, 15 cm and 20 cm) are analysed. Models details in terms of geometry and material are also presented. Results and discussion of finite element analysis using light weight concrete that fulfill important practical requirements are also presented.
- Chapter 8 closes the study with conclusion and a list of recommendations.

CHAPTER 2
LITERATURE REVIEW

2.1 Shell Structures

Shell structures are curved and warped or folded surfaces whose thicknesses are small compared to their other dimensions (Christiansen, 1987). Shells are highly efficient structures that possess several merits over conventional engineering structures of linear geometrical shapes. Shell structures of different shapes and materials are widely applied to serve many purposes. Besides their application as efficient roofing systems covering huge spaces, shells are also found in many industrial and engineering products such as ship hulls, car bodies, aircraft bodies, pipes, piles, dams, tunnels, off shore structures, chimneys, towers, bridges, storage tanks and pressure vessels. Concrete is the most widely used material in shell construction; however other materials have also been used such as welded steel plates, metal decking, plywood, multiple layer timber decks, and fiberglass-reinforced plastic.

Man-made as well as natural surface structures can be broadly classified into two categories namely ‘flexible shells’ and ‘rigid shells’ (Schueller, 1996). Flexible, lightweight tensile membrane structures fall under the first category. Rigid shells are further classified as thin and thick shells, thin shells resist loads in pure membrane and shear action whereas thick shells provide flexural stiffness.

In view of the inspiring source of this study and the associated doubly curved surface with folds, this chapter covers shell or surface structures in general, folded surface/plate structures and a review on the recent works carried out on folded plates and folded plate structures.

2.1.1 Shell Structures in Nature

Shapes, mechanisms and processes found in nature have always been a rich source of inspiration for many technological and engineering successful applications. The inherent complicated multilevel behaviour, with respect to shape and material, of

natural systems in their adaptive response towards external environmental impacts that in many cases are harsh is difficult to understand at a full scale. Geometry in nature has always been the focus of many researchers who tried to understand and interpret conformity and order of proportions employing numbers, lines, surfaces and shapes. Many natural phenomena in plants and animals can be explained with the help of Fibonacci numbers, some examples are spirals of shells, number of petals on some flowers, and leaf arrangement in plants (Knott, 2006).

Schueller (1996) discussed surface structures in nature both at the micro-level as well as the macro-level. At the microscopic level, we have skeletal shell structures of the diatoms (marine algae) and radiolaria (unicellular organisms). These skeletons occur in countless number of shapes and surface structures that disclose complex and delicate geometry. They illustrate nature's correspondence to architectural constructions; they also illustrate nature's implementation of the concept of basic building blocks such as using minimum solid ribs targeting least weight; properties of triangulated, stressed-skin shells are found in some radiolaria. On the other hand, shells of eggs, snails, turtles, mussels, skulls, animal's hollow horns (e.g. goat, sheep), clay nests of ovenbirds, nests of weaverbirds, seashells, plant leaves, etc. are among nature's surface structures at the macro-level (Fig. 2.1).

The above mentioned surface structures represent just a little of nature's collection which inspired many research work particularly at the macro-level. Choong and Voon (2005) studied the shape of the egg shell through investigating the strength and rigidity versus shells of elliptical and spherical shapes. The ample spiral shapes of seashells have always been the focus of many researchers as can be seen from the work of Jirapong and Krawczyk (2003); Selcuk *et al*. (2005); Fowler *et al*. (1992); Lim 2003). Studies related to botanical surfaces considered several aspects such as photosynthesis process, mechanisms, shape influence on the structural behaviour and 3D geometry modeling. Gust (1996) focused on the photosynthesis process for solar energy harvesting, medical imaging and many other applications. De Focatiis and

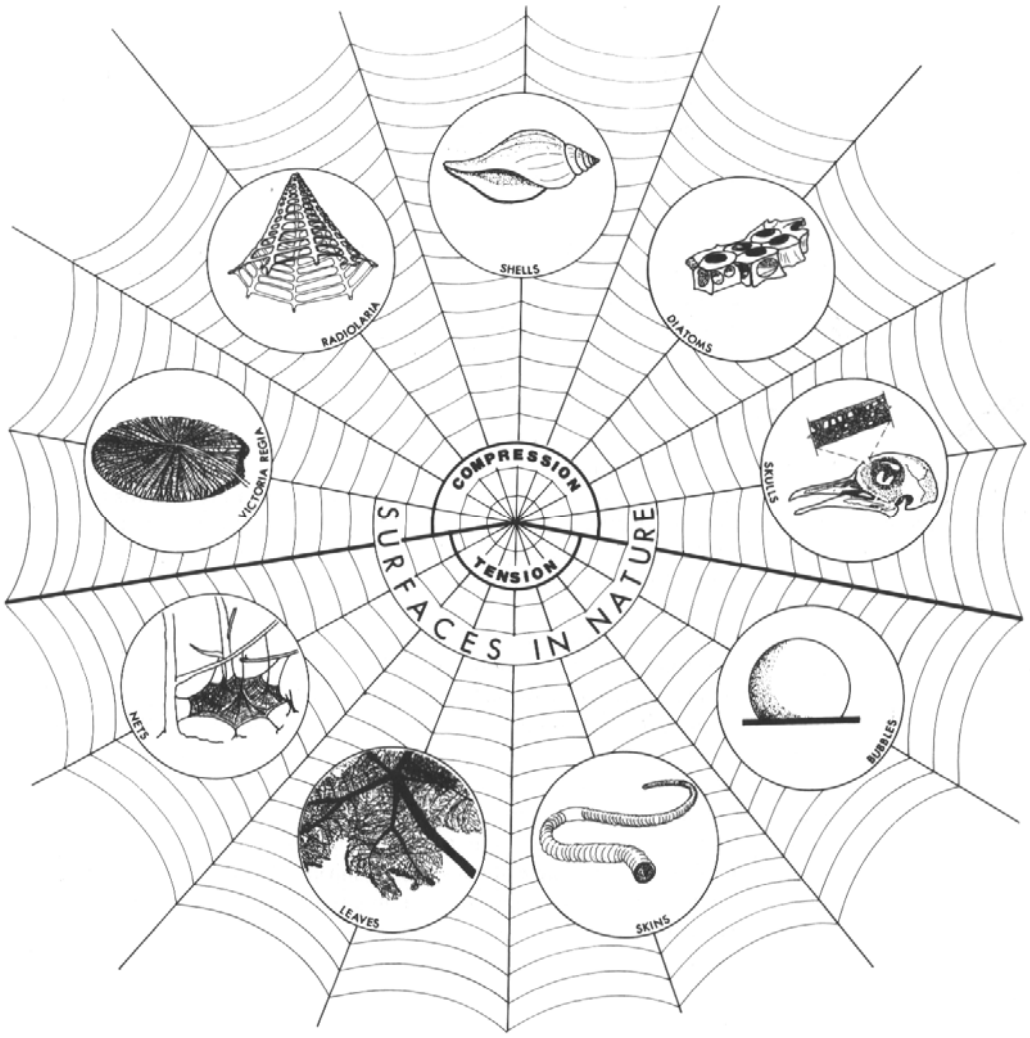

Fig. 2.1: Surfaces in Nature (Schueller, 1996)

Guest (2002); Kobayashi *et al*. (1998) focused on the folding mechanism aspects of some plant leaves for applications like deployable structures such as membranes and tents, solar panels and light weight antennae and satellites. King and Vincent (1996) studied the influence of a leaf shape in terms of curl and fold on its structural stiffness; Ng (2003) modeled the folded surface of the leaf of *J. altifrons* to study the structural merits of this beautiful shell surface in presence of folds – further elaboration in relation to the current study is given in Section 2.4; Balz and Güring (2001) introduced the idea of deployable or temporary structures – made of membrane and erected with air or water pressure - based on the shape stability behaviour of the petal shapes of orchids. Dimian (1997) introduced a solution for generating computer based models of folded leaves of different shapes.

Continuing technological advancements enabled scientists and engineers to unveil secrets of more biological systems for mimicking purposes. However, we still remain limited in transferring the aspects we learn in the way they exactly take place in nature. *Mimosa pudica* is a folding plant with leaves formed of very tiny leaflets that fold rapidly when touched (Armstrong, 2006); on the other hand lies the plant leaves that curl, fold and add material where necessary to withstand the wind effects and to expose as much surface area as possible to light for the vital photosynthesis process (King and Vincent, 1996). The first example reveals an instantaneous natural response to external impacts whereas the second example reveals a response that takes place over a longer period of time. However, despite the advancements made in the analysis, design, material development, and manufacturing or construction methods, we remain far from being able to design structures that can show such a response. When we design, very often we consider the worst load case scenario a structure might face and place material that can sustain the likely adverse effects accordingly. Selection is always made based on suitable shape that remains the same throughout the life time of the structure; we are not yet able to design structures that can alter shape and/or add material where and when needed like the dynamic response of natural systems.

2.1.2 Characteristics of Surface Structures

A surface structure, be it rigid or flexible, is a form resistant structure such as folded plates, rigid shells and tensile membranes (Christiansen, 1987). This is the main feature that discerns surface structures from the conventional skeletal ones. Although, a pressure-vessel is made of physical components that are riveted, bolted or welded together, yet the overall structure has to be of continuous nature to contain a fluid at pressure. The ancient masonry dome or vault is not continuous at the level of its individual building blocks that may not necessarily be cemented together, yet the overall dome structure is in a state of continuous compression that holds the separate masonry blocks together. It is to be highlighted that the *structural continuity* of surface

structures is displayed through their ability in transmitting forces in different directions within the surface of the shell. On the other hand, *skeletal structures* such as braced frames transmit the forces along their individual structural components e.g. beams and columns (Calladine, 1983).

A shell or surface structure is a term that is inherently related to nature expressing the characteristic of dynamic response found in natural systems. The soap film and the natural flowing surface of a suspended membrane are among the driving forces in shaping many of the successful engineering surface structures (refer Section 1.2.1). These natural phenomena lead to minimal surface structures with economy in material and energy. In order to remain in tension, flexible membrane structures change shape in response to changes in live load. Surfaces obtained on flow principles (Billington, 2003); (Lewis, 2005) are in pure tension when hanging; an inverted frozen version of same become surface structures under pure compression. However, certain shapes of rigid shells result in compression, tension as well as tangential shear stresses. Tension in concrete shells can be taken care of by suitable steel reinforcement. A full compression response can be achieved through prestressing the shell. To avoid bending, direct shear and torsion a shell has to be quite thin e.g. egg shell; yet it has to be thick enough to avoid any buckling. Doubly curved thin shells show outstanding structural behaviour to withstand uniform loading in direct force action within its surface plane (Schueller, 1996). Presence of folds on a thin shell surface imparts high structural performance as demonstrated by the natural folded surface of the *J. altifrons*.

A shell should not necessarily be a continuous solid surface. It may take the form of precast ribbed shell units with very thin panels or may be a network of members (Schueller, 1996). The leaf of *J. altifrons*, considered in this study, is a discontinuous doubly curved folded surface; the thin curved strips between successive ridge and valley lines may be visualized as long continuous shell strips which, at a smaller scale, may assumed to be a curved assembly of flat plate elements in a row.

Reinforced concrete, wood, steel, aluminum, plastic and ceramic are the most widely used materials in making surface structures. In case of reinforced concrete surface structures, material cost is relatively low; the very high span to thickness ratio of shells, compared to skeletal structures, render them very economical in terms of material cost. The complicated shape of shells, compared to conventional prismatic skeletal elements, is the dominating cost factor especially in countries where labour cost is high. Shells generally require labour intensive formwork to shape the end product. Reinforced concrete surface structures consisting of self supporting parts can be constructed using segmental type reusable formwork (Schueller, 1996).

2.1.3 Advantages of Shell Structures

Structural simplicity, significance of form and structural economy and safety are major advantages of shells. The thin continuous nature of shell element between inside and outside the structure leads to the same internal and external shape; this shape has to follow strict laws of static in order to be both safe and economical. The natural outstanding strength of shell structures is a function of their curved shape and membrane action; synclastic shells (domes) and anticlastic shells (hyperbolic paraboloids) are strong thin shells of wide application. Shell structures are very useful to span huge areas where internal supports are not desirable to provide large open, unobstructed interior spaces. Highly efficient thin shells result in material economy, remarkable reduction in cost is achieved in case of concrete shells; the very special characteristic of concrete, being inexpensive and easily cast into compound curves render them very suitable and highly economical in shell construction. Reinforced concrete shells, when properly designed and constructed, show outstanding strength and safety. Monolithic domes were reported to resist hurricanes and fires; and are

widely considered to be strong enough to withstand F5 tornadoes* (Wickipedia, 2007a).

2.1.4 Behaviour of Shell Structures

Shells are characterized by their three dimensional load-carrying behaviour determined by their geometry, boundary and support conditions, and the nature of the applied loads. Simplified structural behaviour of shell structures is derived through modeling a shape that will transfer the applied loads into direct forces in the middle surface of the shell called a membrane surface. Stresses in the membrane surface are membrane state of stresses that does not include bending about any axis in the shell (membrane hypothesis). In-plane compressive and shear forces are likely to develop, hence a shell must have some stiffness in order to remain stable and retain its shape. Shells are usually bounded by supporting members and edge members, provided to stiffen the shell and distribute or carry loads in composite action with the shell (Christiansen, 1987). Static equilibrium of shells according to the membrane hypothesis considering all bending, twisting and normal shear-stress resultants to be zero throughout the shell is dealt with in detail by (Calladine, 1983). Methods of preliminary design of different kinds of shells and folded plates along with some examples were given by Ketchum (1987).

In contrast to the simplified behaviour based on the membrane hypothesis, loads on shells are carried by a combination of ‘stretching’ and ‘bending’ action in general (Calladine, 1983). Treatment of the subject of shell behaviour considering these two effects are given in Billington (1982); Calladine (1983). The approach has been based on considering two distinct surfaces that are arranged to sustain the ‘stretching’ and ‘bending’ stress resultants, respectively. The stretching surface has been considered to be identical to a shell analysed according to the membrane

* According to **Fujita scale**, or **Fujita-Pearson scale**, F5 tornado is classified as a violent tornado of potential damage with a speed range of 216-318 mph (416-510 km/h). It shows terrific power in destroying frame structures, debarking trees and badly damaging reinforced concrete structures.

hypothesis whereas the behaviour of the bending surface has been closely related to that of a flat plate.

Fig. 2.2 shows a shell element under normal and tangential loading of intensity *p, q_x and q_y*. N_x and N_y are the membrane direct forces whereas N_{xy} and N_{yx} are the membrane shear forces. On the other hand, Q_x and Q_y are the out of plane shear whereas M_x, M_y, M_{xy} and M_{yx} (=M_{xy}) are the out of plane bending moments and twisting moments, respectively.

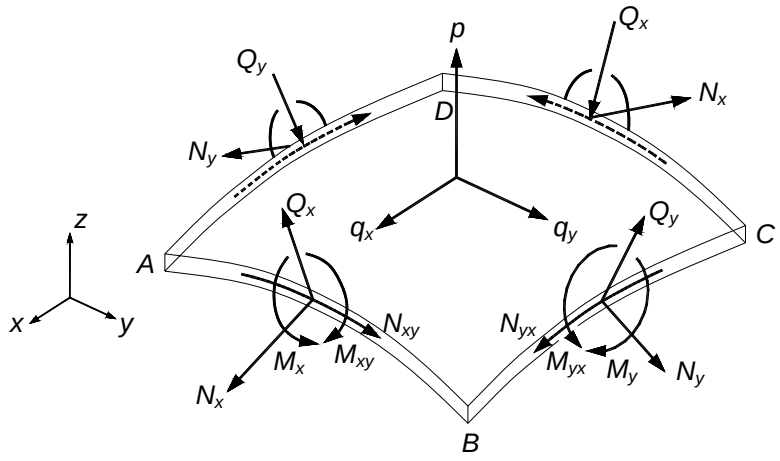

Fig. 2.2: In-Plane and Out of Plane Forces on a Shell Element (Calladine, 1983)

2.1.5 Classification of Shell Systems

Shell systems are generally classified based on two main features namely Gaussian curvature and geometrical shapes.

Classification based on Gaussian curvature is illustrated in Fig. 2.3. *Synclastic* shells are formed by two families of bent lines curving in the same direction, also known as shells of positive Gaussian curvature such as spherical domes and elliptic paraboloids. Shells formed by only one family of curves are shells of zero Gaussian curvature; some examples are cylinders and cones. Shells formed by two families of curves each in opposite direction are called *anticlastic* shells; these are shells of negative Gaussian curvature such as hyperbolic paraboloids and hyperbolas of

revolution. Gaussian curvature (*K)* of a surface is a function of the principal curvatures of the curves generating that surface as illustrated by Eq. 2.1 (Billington, 1982).

$$K = \frac{1}{r_x}\frac{1}{r_y} \quad \text{----------} \quad \text{Eq. 2.1}$$

where r_x and r_y are the radii of curvature of the adjacent sides of the shell (Fig. 2.3).

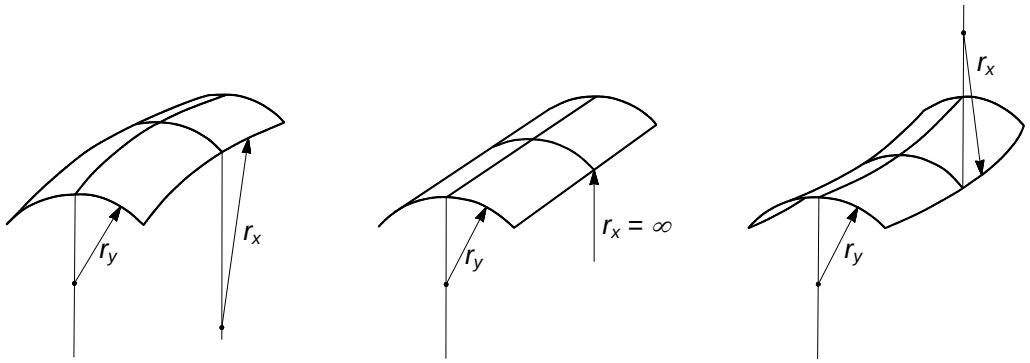

Fig. 2.3: Definition of Curvature (Billington, 1982)

The other useful classification categorizes shells into rotational and translational systems. A surface generated by translating a plane curve over another plane curve is a shell of translation (Fig. 2.4(a)); some examples are elliptic paraboloids and hyperbolic paraboloids. On the other hand, a plane curve rotated about an axis lying in the plane of the curve generates a shell of revolution such as domes and cylindrical tanks (Fig. 2.4 (b)). Classification of shell structures by geometry is given in Table 2.1.

In view of the above classification systems, we observe that the surface of the leaf of *J. altifrons* cannot, distinctively be placed in either of the above mentioned categories. In fact the *J. altifrons* is a combination of doubly curved surface (synclastic or anticlastic) surface with approximately parallel folds extending from the central spine (Figs. 1.2, 1.3 and 1.4). As such, this beautiful combination of surfaces presented by nature, perhaps, partially contributed for such leaves to sometimes grow to a height of